J Mater Sci: Mater Electron (2023) 34:2216

Emission spectroscopy of Sm^{3+} ion-activated zinc phosphate glass for reddish-orange lighting applications

S. Vidya Sagar[1], S. Babu[2], and K. Venkata Rao[1,*]

[1] *Dept. of Physics, Government Degree College, Porumamilla, Kadapa, A.P 516193, India*
[2] *Dept. of Physics, Rajeev Gandhi Memorial College of Engineering & Technology, Nandyal, A.P 518501, India*

Received: 10 August 2023
Accepted: 6 November 2023

© The Author(s), under exclusive licence to Springer Science+Business Media, LLC, part of Springer Nature, 2023

ABSTRACT

This work focuses on studying the photoluminescence properties of Sm^{3+} ion-activated zinc phosphate (ZnP) glasses for visible reddish-orange illumination applications. A conventional melt-quenching method was used to synthesize ZnP glasses with (60-x) P_2O_5–20ZnO–10LiF–10SrO–xSm_2O_3 compositions, where x = (0.1, 0.5, 1.0, 1.5, and 2.0). Structural characterization by X-ray diffraction (XRD) confirmed the amorphous nature of the synthesized glasses, whereas Fourier-transform infrared spectroscopy (FTIR) revealed characteristic phosphate groups. The optical properties were assessed using absorption and photoluminescence spectroscopy, along with decay-lifetime measurements. Applying the Judd–Ofelt (J–O) theory, the spectral intensities (f_{emp} and f_{qun}) and intensity parameters (Ω_2, Ω_4, and Ω_6) were derived from the absorption spectra, showing a trend of $\Omega_4 > \Omega_6 > \Omega_2$. From the obtained J–O parameters, the radiative parameters (A_T and τ_R) were estimated for various excited states. Photoluminescence analysis showed four emission bands corresponding to the $^4G_{5/2} \rightarrow {}^6H_{P/2}$ (P = 5, 7, 9, and 11) transitions of Sm^{3+} ions when stimulated at 403 nm, with a strong reddish-orange emission intensity at 599 nm. The stimulated emission cross-sections (σ_P) were estimated from the emission spectra. Chromaticity color coordinates confirmed that ZnP glasses doped with Sm^{3+} ions show reddish-orange luminescence and are useful for potential reddish-orange lighting applications.

1 Introduction

Glass and glass-like materials are often used in breakthrough technologies due to their characteristic structure and optical properties [1]. These materials are recognized for their high density, toughness, moisture resistance, high transparency, environmental friendliness, non-toxicity, and harmlessness to health [2–4]. There are many industrial and technological applications, such as large-scale architectural glazing and roll-to-roll manufacturing processes to produce flexible displays, solar modules, photovoltaic devices, and field lighting systems [5].

Address correspondence to E-mail: drvenkataraok@gmail.com

https://doi.org/10.1007/s10854-023-11608-y
Published online: 24 November 2023

In the last few decades, RE-doped glasses have been named instead of crystals or ceramics [6]. Their many applications, such as solid-state lasers [7], waveguide lasers for optical communications, solar cells, photonic devices, and 3D displays, have attracted attention [8]. Oxide glasses, including luminous rare earth ions (RE), have attracted considerable attention because of their remarkable optical properties, high thermal and chemical stabilities, and high conversion efficiencies [9, 10].

Many studies have been conducted on phosphate glasses (P_2O_5) owing to their low melting points, good alkali and lanthanide ion solubility, dispersion, high gain density, and good transmittance in the ultraviolet (UV) region [11, 12]. Owing to their distinctive and appealing spectral features in the UV–VIS–NIR range, phosphate glasses activated with RE elements are used in several applications including luminous materials and optical amplifiers [13]. Phosphate glasses are used in various industrial applications including biomedical materials, lasers, and solid-state electrolytes [13].

Samarium (Sm^{3+}) was chosen as the dopant or active center in this study, and phosphate (P_2O_5) was chosen as the glass matrix. Samarium was chosen as the optically active center because of its outstanding visible fluorescence, reduced non-radiative decay, strong reddish-orange luminescence originating from the $^4G_{5/2}$ level [14], high quantum efficiency, low quantum defects, and promising spectrum hole-burning properties [15]. Sm^{3+}-containing glasses have recently gained attention because of their possible use in color displays, undersea communications, and high-density optical storage [16]. In addition, intermediate formers, and modifiers, such as ZnO, SrO, and LiF, are added to the glass composition to mitigate several drawbacks of phosphate, such as its hygroscopic nature and low chemical resistance. Zinc oxide (ZnO), an excellent glass modifier, can enhance the chemical resistance of phosphate glasses because of its P–O–P bonds [17]. Lithium fluoride (LiF) is added to glass to keep its transparency [18]. Strontium oxide (SrO) is an alkaline earth oxide and good glass modifier [19].

Selected ZnP glasses doped with Sm^{3+} ions are particularly helpful for laser media because of their highly visible emission (reddish-orange luminescence), broad energy levels, prolonged metastable decay time, high photoluminescence intensity, increased stimulated emission cross-section, and high quantum efficiency [5, 6, 18]. In addition, glasses doped with Sm^{3+} ions can be used in various applications, including compressed fiber lasers [19], color displays, bio-friendly light sources, microbeam radiotherapy, optical amplifiers, luminescence down-switching in solar cells, hole burning [20], planar waveguides, optical storage devices, and high-density optical devices [21].

In recent years, researchers have extensively studied various glass matrices doped with Sm^{3+} ions. Recently, Yamusa et al. [22] explored the spectral and radiative features of barium sulfoborophosphate glasses activated with trivalent Sm^{3+} ions using Judd–Ofelt theory. Non-crystalline SiO_2–SrO–MgO glasses activated with trivalent Sm^{3+}ions and co-doped trivalent Sm^{3+}/Dy^{3+} $Sr_2MgSi_2O_7$ glass–ceramics were studied by Fernandez-Rodriguez et al. for their thermal, structural, and spectral features [23]. According to Ataullah et al., lithium telluride-based glasses with trivalent Sm^{3+} ions exhibit spectral characteristics suitable for orange-lighting applications [24]. In their study of orange laser applications, Bayoudhi et al. examined the spectroscopic properties of undoped and Sm^{3+} ion-doped P_2O_5–Na_2O–Al_2O_3–BaO glasses [25]. Lakshminarayana et al. fabricated and examined the fluorescence properties of borate glasses with alkali oxides activated using a trivalent Sm^{3+} ion concentration of 1 mol% for orange LEDs [26]. According to Sailaja et al., Sm^{3+} ion-doped oxy chloro boro tellurite glasses have optical properties suitable for reddish-orange laser applications [27]. Siva Raju et al. for photonic applications, concentration quenching effect on luminescence properties of ZnBiNaPsr glasses doped with Sm^{3+} ions studied [28]. This study focuses on analyzing the photoluminescence properties of Sm^{3+} ion-activated ZnP glasses for visible reddish-orange lighting applications.

2 Materials and methods

2.1 Sample preparation

The melt-quenching method was used to synthesize ZnP glasses with a (60-x)P_2O_5–20ZnO–10LiF–10SrO–xSm_2O_3 composition, designated as xSmZnP, where x = (0.1, 0.5, 1.0, 1.5, and 2.0). Each of these ZnP glasses was named as 0.1SmZnP, 0.5SmZnP, 1.0SmZnP, 1.5SmZnP, and 2.0SmZnP as listed in Table 1. Phosphorus pentoxide (P_2O_5), lithium fluoride (LiF), zinc oxide (ZnO), strontium oxide (SrO), and samarium oxide (Sm_2O_3) with a purity of 99.99% are used as raw materials. The ingredients were combined, weighed according to their composition, ground using an agate mortar, transferred to an

Table 1 Glass code and Composition of the zinc phosphate (ZnP) glasses doped with different concentrations of Sm^{3+} ions

S. No	Glass code	Composition (mol%)
1	0.1SmZnP	$59.9P_2O_5+20ZnO+10SrO+10LiF+0.1Sm_2O_3$
2	0.5SmZnP	$59.5P_2O_5+20ZnO+10SrO+10LiF+0.5Sm_2O_3$
3	1.0SmZnP	$59.0P_2O_5+20ZnO+10SrO+10LiF+1.0Sm_2O_3$
4	1.5SmZnP	$58.5P_2O_5+20ZnO+10SrO+10LiF+1.5Sm_2O_3$
5	2.0SmZnP	$58.0P_2O_5+20ZnO+10SrO+10LiF+2.0Sm_2O_3$

aluminum crucible, and heated at an elevated temperature of 1150 °C for 1 h in a furnace. After quenching on a brass plate, the molten liquid was pressed through a second brass plate. To remove the internal tension, the samples were annealed for 3 h at 300 °C. The samples were annealed, allowed to cool to ambient temperature, and then subjected to various characterizations.

The density (ϱ) and refractive index (η) of the Sm^{3+}-doped ZnP glasses were measured. Deionized water was used as the immersion medium to determine density (ϱ). Using an Abbe ATAGO digital refractometer and $C_{10}H_7Br$ as the contact liquid, the refractive index (η) of the glass samples was figured out. The amorphousness of Sm^{3+} ion-doped ZnP was analyzed with a Rigaku Mini Flex 600 X-ray diffractometer (XRD) using Cu K(alpha) radiation operating at 40 kV and 15 mA in the range of 10–70° with a step size of 0.02°. A Bruker Compact FTIR Spectrometer (Alpha II) was used to obtain FTIR spectra in the range of 400–4000 cm^{-1} using the KBr pellet method. Optical absorption spectra were recorded using a Jasco V570 spectrophotometer with a resolution of 1.0 nm in the range–200–1800 nm. Excitation, emission, and lifetime data were recorded by Horiba Fluorolog-3 fluorescence with TCSPC at 0.2 nm resolution and a 450 W broadband xenon arc lamp as the light source.

2.2 Judd–Ofelt hypothesis and radiative parameters

Based on Judd–Ofelt (J-O) theory, empirical (f_{emp}) and quantified (f_{qun}) spectral intensities were obtained using Eqs. (1) and (2), respectively [24].

$$f_{emp} = 4.32\times10^{-9}\times\int \varepsilon(\upsilon)d\upsilon \tag{1}$$

where $\varepsilon(\upsilon)$ is the corresponding absorption band's molar absorption coefficient at wave number $\upsilon(cm^{-1})$.

$$f_{qun}(\varphi P\rightarrow\varphi' P') = \frac{8\pi^2 mc\upsilon}{3he^2(2J+1)}\times\frac{(\eta^2+2)^2}{9\eta}\Big[\sum_{\lambda=2,4,6}\Omega_\lambda \left\langle \varphi P \parallel U^\lambda \parallel \varphi' P'\right\rangle^2\Big] \tag{2}$$

where $\sum_{\lambda=2,4,6}\Omega_\lambda\left\langle \varphi P \parallel U^\lambda \parallel \varphi' P'\right\rangle^2$ is the line strength of the electric dipole transition, P and P′ are the total angular momentum of the ground state and excited states, respectively, h is the Planck constant(6.6260×10^{-34}), and η is the refractive index, $\|U^\lambda\|^2$, is reduced matrix elements and $\Omega_\lambda(\lambda=2,4,6)$ is Judd–Ofelt intensity parameter.

$$\Omega_\lambda = \left[1.0847\times10^{11}\times(\eta^2+2)^2/9\eta\right]^{-1}\times(2P+1)\times T_\lambda \tag{3}$$

The root means square deviations δ_{RMS} of the empirical (f_{emp}) and quantified (f_{qun}) spectral intensities were obtained using the following equation:

$$\delta_{RMS} = \sum\sqrt{\frac{(f_{emp}-f_{qun})^2}{N}} \tag{4}$$

where, N is the number of transitions.

The following equations were used to calculate the lifetimes(τ_R) and probabilities (A_R) of radiative transitions:-

$$A_R(\varphi P,\varphi' P') = \frac{64\pi^4\upsilon^3e^2}{3h(2P+1)}\left\{\frac{\eta(\eta^2+2)^2}{9}S_{ED}+\eta^3 S_{MD}\right\} \tag{5}$$

where S_{ED} and S_{MD} are the electric and magnetic dipole line strength, respectively.

The calculated radiative lifetime (τ_R) is the inverse of the sum of the probabilities of radiative transitions (A_R):

$$\tau_R = \frac{1}{\sum A_R(\varphi' P')} \tag{6}$$

The stimulated emission cross-section (σ_P) was calculated using the Füchtbauer-Ladenburg equation [8, 24]:

$$\sigma_P(\varphi P, \varphi' P') = \frac{\lambda_p^4 \times A_R(\varphi P, \varphi' P')}{8\pi c\eta^2 \times \Delta\lambda_{eff}} \quad (7)$$

where λ_P is the wavelength of the emission peak, and $\Delta\lambda_{eff}$ is the effective bandwidth of the corresponding emission.

2.3 CIE 1931 color coordinates

The CIE1931 color chromaticity diagram uses the emission spectra to figure out the three chromaticity coordinates (x, y, and z) that describe the emission color. The correlated color temperature (CCT) of the light source can be found from its CIE 1931 x-, and y-chromaticity values. A common method for calculating CCT is the McCamy approximation [12, 29].

$$CCT = 437n^3 + 3601n^2 + 6861n + 5517 \quad (8)$$

where

$$n = (x_c - 0.332)/(y_c - 0.186).$$

where x_c and y_c are the chromaticity coordinates of the light source in the CIE 1931 color space.

Color purity, on the other hand, is a measure of how pure a color is, and is free from any mixture of other colors. It was calculated from the chromaticity color coordinates x_c and y_c in the CIE 1931 color space, using the following formula:

$$CP(\%) = \frac{\overline{NC}}{\overline{ND}} \times 100 \quad (9)$$

where $\overline{NC}$ is the distance between the neutral point ($x_n = 0.3101, y_n = 0.3162$) and color coordinates (x_c, y_c). $\overline{ND}$ is the distance between the neutral point (x_n, y_n) and the dominant wavelength coordinates (x_{dom}, y_{dom}).

3 Results and discussion

3.1 Physical properties

As presented in Table 2, for the 0.1, 0.5, 1.0, 1.5, and 2.0 mol% Sm^{3+} ion-doped ZnP glasses, the refractive indices were 1.643, 1.645, 1.649, 1.655, and 1.656, respectively. The density values (ρ) for 0.1, 0.5, 1.0, 1.5, and 2.0 mol% Sm^{3+} ion concentrations were 2.516, 2.548, 2.565, 2.576, and 2.597 g/cm^3, respectively. As shown in Fig. 1, the refractive index and density of the ZnP glasses doped with Sm^{3+} ions increased with increasing Sm^{3+} ion concentration.

3.2 XRD analysis

The XRD profiles of ZnP glasses doped with different concentrations of Sm^{3+} ions are shown in Fig. 2. The patterns were broad with no sharp crystalline peaks, indicating the amorphous nature of the prepared ZnP glasses. The XRD profiles confirmed that the ZnP

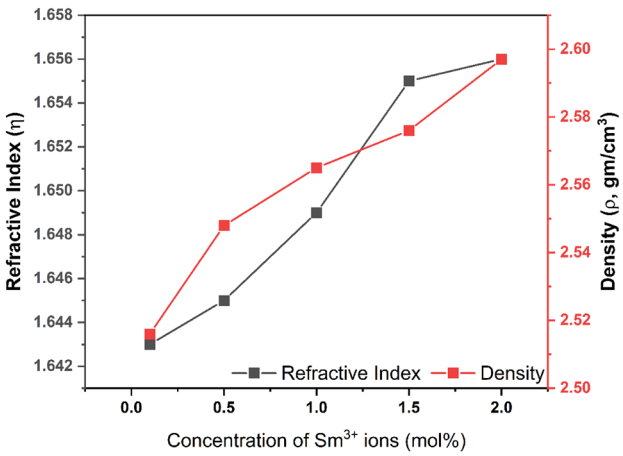

Fig. 1 Variation of refractive index and density with different concentration of Sm^{3+} ions (mol%) (Color figure online)

Table 2 Physical and optical parameters of the investigated zinc phosphate glasses doped with Sm^{3+} ions

Parameter	0.1 SmZnP	0.5 SmZnP	1.0 SmZnP	1.5 SmZnP	2.0 SmZnP
Thickness (t, cm)	0.763	0.687	0.413	0.325	0.382
Refractive index (η)	1.643	1.645	1.649	1.655	1.656
Density(ρ, gm.cm^{-3})	2.516	2.548	2.565	2.576	2.597
Molecular weight (M)	114.59	115.41	116.45	117.49	118.51
RE Ion concentration (N×10^{20}, ions. cm^{-3})	0.132	0.664	1.326	1.980	2.639
Inter ionic distance (r$_i$×10^{-07} Å)	4.231	2.469	1.961	1.715	1.559

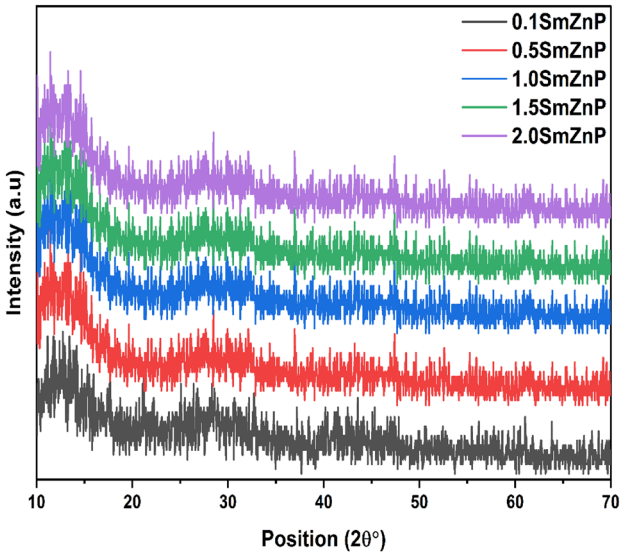

Fig. 2 XRD profiles of zinc phosphate (ZnP) glasses doped with different concentrations of Sm^{3+} ion (Color figure online)

glasses remained amorphous, even after doping with Sm^{3+} ions.

3.3 FTIR spectrum analysis

Figure 3 shows the FTIR spectra of undoped ZnP glass and 2.0 mol% of samarium-doped glass (2.0SmZnP) in the mid-infrared range from 4000 to 400 cm^{-1}. The spectra of undoped ZnP glass and 2.0 mol% of samarium-doped ZnP glass (2.0SmZnP) glass shows ten peaks at wavenumbers ~ 3427, ~ 2925, ~ 2854, ~ 2324, ~ 1623, ~ 1260, ~ 1080, ~ 907, ~ 762, and ~ 529 cm^{-1}, respectively. It can be seen that there is no difference in the number of peaks of undoped ZnP glass and 2.0 mol% of samarium-doped ZnP glass (2.0SmZnP), but the intensity of peaks is varied. P–O–H bonds were observed at approximately 3427 cm^{-1} [19]. The bands at approximately 2925, 2854, 2324, and 1623 cm^{-1} are attributed to hydrogen bonding with OH [19, 24, 30].

The metaphosphate groups show a band at 1260 cm^{-1} due to non-bridging O–P–O bonds superimposed with the asymmetric stretching vibrations of the P=O bonds [10, 19]. The asymmetric stretching vibrations of the PO_2 groups were observed at approximately 907 and 1080 cm^{-1} [10, 19]. The P-O-P bonds are stretched symmetrically at ~ 762 cm^{-1} [10, 19]. The peak at 529 cm^{-1} is associated with O=P–O bending vibrations or harmonics of the P–O–P bond [10, 13, 19].

3.4 Analysis of optical absorption spectra

The optical absorption spectra of ZnP glasses doped with varying concentrations of Sm^{3+} ions are shown in Fig. 4. In the case of samarium ion-doped ZnP glasses, there were five absorption peaks in the UV–visible region and seven in the NIR region. Conversely, the absorption spectrum of the undoped ZnP glass or ZnP glass with 0 mol% concentration did not show any peaks. From Fig. 4, it can be seen that the number of peaks remains constant as the concentration of Sm^{3+} ions increases in the glass composition. However, a

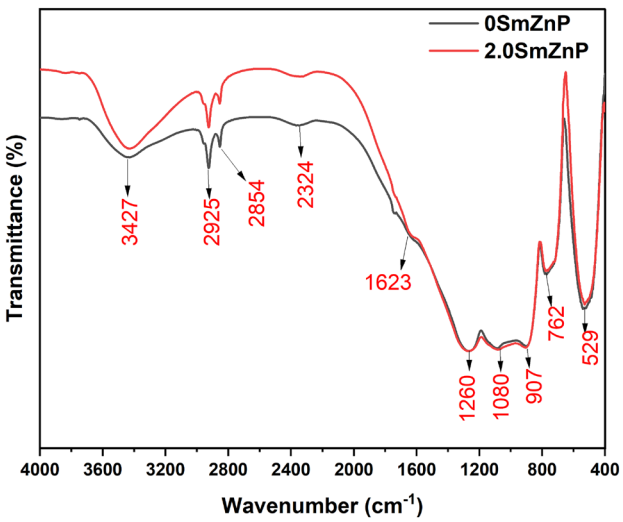

Fig. 3 FTIR spectra of undoped ZnP glass and 2.0 mol% of Sm^{3+} ions doped zinc phosphate (ZnP) glass (Color figure online)

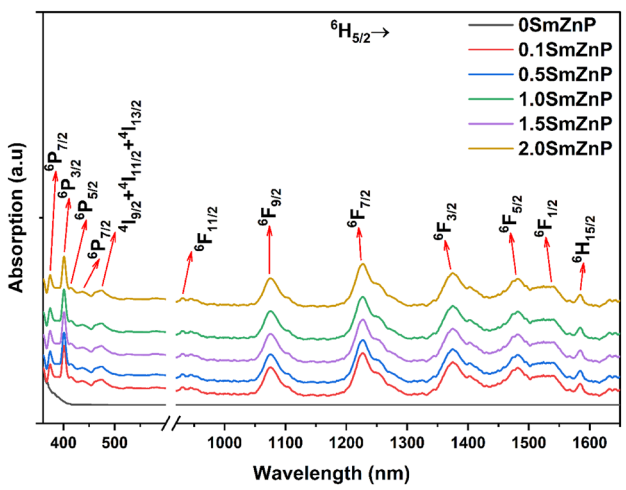

Fig. 4 Absorption spectra of zinc phosphate (ZnP) glasses doped with Sm^{3+} ions (0, 0.1, 0.5, 1.0, 1.5, and 2.0 mol%) (Color figure online)

discernible increase in the intensity of the observed peaks was observed. The observed absorption peaks are named according to their respective wavelengths (376 nm: $^6H_{5/2} \rightarrow {}^6P_{7/2}$), (401 nm: $^6H_{5/2} \rightarrow {}^6P_{3/2}$), (414 nm:$^6H_{5/2} \rightarrow {}^6P_{5/2}$), (438 nm: $^6H_{5/2} \rightarrow {}^4G_{9/2}$), (474 nm: $^6H_{5/2} \rightarrow {}^4I_{9/2} + {}^4I_{11/2} + {}^4I_{13/2}$), (930 nm:$^6H_{5/2} \rightarrow {}^6F_{11/2}$), (1077 nm:$^6H_{5/2} \rightarrow {}^6F_{9/2}$), (1230 nm:$^6H_{5/2} \rightarrow {}^6F_{7/2}$), (1381 nm:$^6H_{5/2} \rightarrow {}^6F_{5/2}$), (1482 nm:$^6H_{5/2} \rightarrow {}^6F_{3/2}$), (1544 nm:$^6H_{5/2} \rightarrow {}^6F_{1/2}$), and (1588 nm:$^6H_{5/2} \rightarrow {}^6H_{15/2}$) using the W.T Carnal and previous reports [5, 9, 31, 32]. The absorption peaks of $^6H_{5/2} \rightarrow {}^6P_{3/2}$ at 401 nm and $^6H_{5/2} \rightarrow {}^6F_{7/2}$ at 1230 nm were more intense than those of the others and showed strong absorption. These absorption bands are known as hypersensitive transitions (HST). The HST transitions of Sm^{3+} ions followed the selection rules such as $|\Delta S| = 0$, $|\Delta J| \leq 2$, and $|\Delta L| \leq 2$, which are sensitive to even slight changes in their surroundings [21]

3.5 Judd–Ofelt (J–O) intensity and radiative parameters

The empirical spectral intensity (f_{emp}) depends on the absorption band area. For each band of the absorption spectra of the ZnP glass doped with Sm^{3+} ions, the oscillator strengths (f_{emp}) and (f_{qun}) were calculated using Eqs. (1) and (2), respectively. Table 3 presents the results. Using Eq. (4), the δ_{RMS} deviation values were determined for the Sm^{3+} ion-doped ZnP glasses in small quantities. The δ_{RMS} deviation was determined as the quality of the linear fit [33]. The fit between f_{emp} and f_{qun} depicts the precision of the J-O intensity parameter and the quality of the fit [33]. Table 3 shows that the spectral intensities of the two absorption bands, $^6H_{5/2} \rightarrow {}^6F_{7/2}$ and $^6H_{5/2} \rightarrow {}^6P_{3/2}$, are more significant. The J–O intensity parameters $\Omega_\lambda (\lambda = 2, 4, 6)$ were obtained using Eq. (3) for all Sm^{3+} ion-doped ZnP glasses and compared with previously reported samarium-doped glasses, which are listed in Table 4. The local structure and asymmetry around the Sm^{3+} ion site affect the Ω_2 parameter, which is related to the covalency [24]. Glass characteristics such as the viscosity and stiffness of the metal–ligand interactions, may be associated with parameters Ω_4 and Ω_6 [24].

In this study, the trend of the J-O intensity parameters in the order $\Omega_4 > \Omega_6 > \Omega_2$ was discovered, and the previously reported glasses SBNCSm01 [21], OCBTSm0.5 [27], PBBiLiT [32], PBBiSrT [32], BiBSm1 [34], and KABPSm5 [35] followed a similar trend. Low Ω_2 values denote low covalency and low asymmetry, whereas high Ω_4 values reflect the stiffness of the related host glass. The Ω_2 parameter was higher in the glass matrix of 1.0SmZnP (0.17×10^{-20} cm^{-2}) and lower in the glass matrix of 0.5SmZnP (0.03×10^{-20} cm^{-2}). The glasses with 0.1SmZnP (6.08×10^{-20} cm^{-2}) and 2.0SmZnP (0.55×10^{-20} cm^{-2}) had higher and lower values of Ω_4, respectively, indicating higher and lower stiffness, respectively.

Equations (5), and (6) were used to compute the radiative characteristics such as the total radiative transition probability rates (A_T) and radiative lifetimes (τ_R), respectively for different excited states of the Sm^{3+} ion-doped ZnP glasses. The results are listed in Table 5. The total radiative transition

Table 3 Empirical and quantified oscillator strengths (f_{emp} & $f_{qun} \times 10^{-6}$) and RMS deviations ($\delta_{RMS} \times 10^{-6}$) of ZnP glasses doped with Sm^{3+} ions (0.1, 0.5, 1.0, 1.5, and 2.0 mol%)

Energy Level	0.1SmZnP		0.5SmZnP		1.0SmZnP		1.5SmZnP		2.0SmZnP	
S'L'J'	f_{emp}	f_{qun}	f_{emp}	f_{qun}	f_{emp}	f_{qun}	f_{emp}	f_{qun}	f_{emp}	f_{qun}
$^6P_{7/2}$	2.15	2.29	0.59	0.59	0.47	0.74	0.58	0.51	0.38	0.29
$^6P_{3/2}$	7.41	7.19	2.10	1.59	1.74	1.55	1.21	1.26	0.78	0.63
$^6P_{5/2}$	0.02	0.03	0.01	0.24	0.00	0.23	0.01	0.19	0.00	0.09
$^4G_{9/2}$	0.26	0.12	0.13	0.03	0.08	0.03	0.04	0.02	0.04	0.01
$^4I_{9/2} + {}^4I_{11/2} + {}^4I_{13/2}$	2.26	2.09	0.83	0.24	0.71	0.30	0.50	0.21	0.33	0.12
$^6F_{11/2}$	0.58	0.73	0.14	0.16	0.07	0.20	0.12	0.14	0.10	0.08
$^6F_{9/2}$	4.09	4.16	0.92	0.99	1.07	1.22	0.76	0.85	0.51	0.48
$^6F_{7/2}$	6.73	6.60	1.49	1.46	1.81	1.70	1.28	1.23	0.64	0.67
$^6F_{5/2}$	3.48	3.40	0.78	0.78	0.79	0.77	0.71	0.62	0.35	0.31
$^6F_{3/2}$	0.78	1.56	0.17	0.35	0.20	0.37	0.12	0.29	0.07	0.15
$^6F_{1/2}$	0.60	0.06	0.14	0.01	0.15	0.04	0.13	0.02	0.07	0.01
$^6H_{15/2}$	0.13	0.04	0.03	0.01	0.03	0.01	0.02	0.01	0.02	0.01
δ_{rms}	±0.30		±0.24		±0.18		±0.12		±0.08	

Table 4 J-O intensity parameters (Ω_2, Ω_4, Ω_6 $\times 10^{-20} cm^2$), trends and spectroscopic quality factor ($\chi = \Omega_4/\Omega_6$) of ZnP glasses doped with Sm^{3+} ions (0.1, 0.5, 1.0, 1.5, and 2.0 mol%) and comparison

Glass code	Ω_2	Ω_4	Ω_6	Trend	$\chi = \Omega_4/\Omega_6$
0.1SmZnP [Present]	0.170	6.080	4.840	$\Omega_4 > \Omega_6 > \Omega_2$	1.26
0.5SmZnP [Present]	0.030	1.400	1.070	$\Omega_4 > \Omega_6 > \Omega_2$	1.31
1.0SmZnP [Present]	0.120	1.360	1.340	$\Omega_4 > \Omega_6 > \Omega_2$	1.02
1.5SmZnP [Present]	0.060	1.110	0.920	$\Omega_4 > \Omega_6 > \Omega_2$	1.21
2.0SmZnP [Present]	0.050	0.550	0.530	$\Omega_4 > \Omega_6 > \Omega_2$	1.05
SBNCSm1 [21]	2.303	8.640	3.561	$\Omega_4 > \Omega_6 > \Omega_2$	2.42
OCBTSm0.5 [27]	0.641	2.411	2.365	$\Omega_4 > \Omega_6 > \Omega_2$	1.01
PBBiLiT [32]	0.015	5.379	3.378	$\Omega_4 > \Omega_6 > \Omega_2$	1.59
PBBiSrT [32]	0.239	7.383	3.717	$\Omega_4 > \Omega_6 > \Omega_2$	1.98
BiBSm1 [34]	1.746	2.975	1.824	$\Omega_4 > \Omega_6 > \Omega_2$	1.63
KABPSm5 [35]	1.800	2.520	1.830	$\Omega_4 > \Omega_6 > \Omega_2$	1.37

Table 5 Total radiative transition rates (A_T s^{-1}) and radiative lifetimes (τ_R μs) of certain excited states of ZnP glasses doped with Sm^{3+} ions (0.1, 0.5, 1.0, 1.5, and 2.0 mol %)

Sample	$^6F_{11/2}$		$^6F_{9/2}$		$^6F_{7/2}$		$^6F_{5/2}$		$^6F_{3/2}$		$^6H_{15/2}$		$^6H_{13/2}$	
	A_T	τ_R	A_T	τ_R	A_T	τ_R	A_T	τ_R	A_T	τ_R	A_T	τ_R	A_T	τ_R
0.1SmZnP	367	02723	1466	0682	1242	0804	932	01072	628	01592	430	02323	280	03573
0.5SmZnP	083	12033	0328	3048	0278	3588	209	04768	142	07052	097	10267	063	15798
1.0SmZnP	089	11148	0386	2586	0322	3098	237	04210	157	06373	106	09381	069	14388
1.5SmZnP	068	14598	0277	3611	0234	4271	175	05714	118	08496	081	12330	053	18868
2.0SmZnP	036	27855	0154	6489	0129	7764	095	10537	063	15848	043	23202	028	35461

probability rates (A_T) were higher for lower concentrations of Sm^{3+} ions (0.1SmZnP) and lower for higher concentrations of Sm^{3+} ions (2.0SmZnP) and the radiative lifetimes (τ_R) were vice-versa to the total radiative transition probability rate (A_T). The $^6F_{11/2} \rightarrow {}^6F_{9/2}$ transition had the highest total radiative transition probability (A_T) for all the glasses, showing strong radiative emission. The radiative lifetime (τ_R) of the $^6H_{15/2} \rightarrow {}^6H_{13/2}$ transition was the highest for all the glasses, implying a long-lived metastable state.

One of the most crucial laser characteristics used to assess stimulated optical emission in an active medium is the quality factor (χ), which is the ratio of Ω_4 to Ω_6 [27]. The magnitude of the quality factor (χ) explains the stimulated emission in ZnP glasses doped with Sm^{3+}ions. In the present glasses, these values are 1.26, 1.31, 1.02, 1.21, and 1.05 for 0.1SmZnP, 0.5SmZnP, 1.0SmZnP, 1.5SmZnP, and 2.0SmZnP glass matrices, respectively, and the previously described glasses OCBTSm0.5 [27], SBNCSm01 [21], PBBiLiT [32], PBBiSrT [32], BiBSm1 [34], and KABPSm5 [35] have quality factors of 1.01, 2.42, 1.59, 1.98, 1.63, and 1.37, respectively, so the results obtained are consistent with previous reports. An active medium with a quality factor greater than one is considered a suitable candidate for lasing [27]. According to these results, zinc phosphate glass (ZnP) doped with Sm^{3+} ions is a suitable candidate for laser media.

3.6 Excitation and emission spectra

Figure 5 shows the excitation spectra of the ZnP glasses doped with Sm^{3+} ions at a fixed emission wavelength of 599 nm in the 300–550 nm range. By the intra-configurational (f–f) transitions of Sm^{3+} ions [5, 36, 37], the spectra display ten different excitation bands, as illustrated in Fig. 5. These bands are observed at ~ 346, ~ 362, ~ 376, ~ 403, ~ 418, ~ 438, ~ 462 , ~ 476, ~ 501, and ~ 528 nm, corresponding to transitions from ground state $^6H_{5/2}$ to various excited states $^4H_{9/2}$, $^4D_{1/2}$, $^6P_{7/2}$, $^4F_{7/2}$, $^4M_{19/2}$, $^4G_{9/2}$, $^4I_{13/2}$, $^4I_{11/2}$, $^4G_{7/2}$, and $^4F_{3/2}$, respectively [5]. Among these transitions, the $^6H_{5/2} \rightarrow {}^4F_{7/2}$ absorption transition at 403 nm showed a particularly high intensity. A wavelength of 403 nm

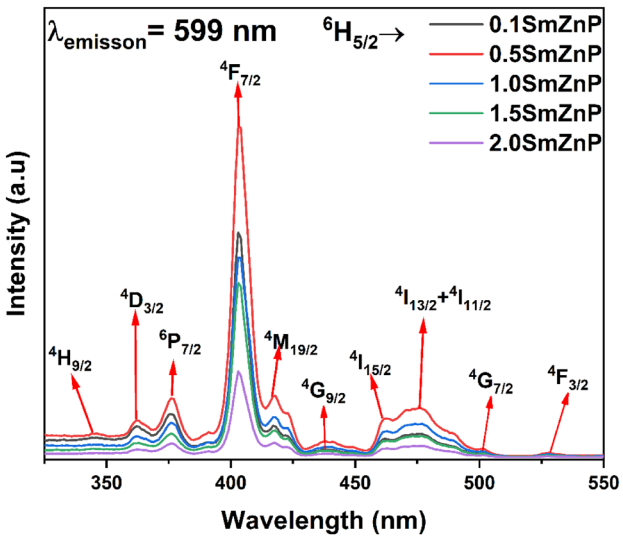

Fig. 5 Excitation spectra of zinc phosphate (ZnP)glasses doped with Sm^{3+} ions (0.1, 0.5, 1.0, 1.5, and 2.0 mol%) in the 300–550 nm region (Color figure online)

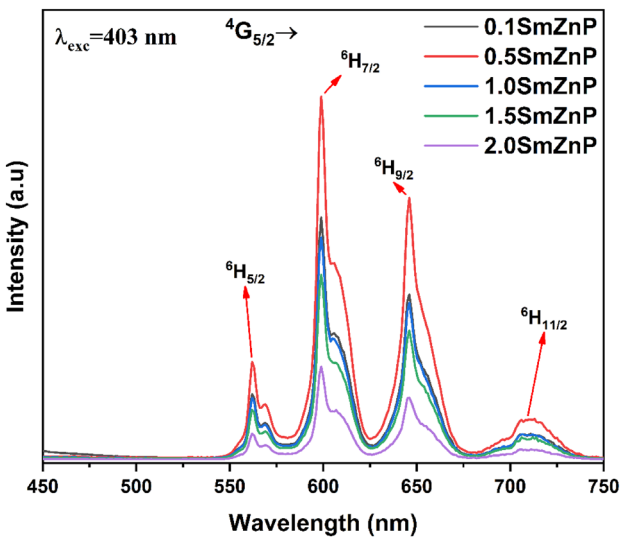

Fig. 6 Emission spectra of zinc phosphate (ZnP)glasses doped with Sm^{3+} ions (0.1, 0.5, 1.0, 1.5, and 2.0 mol%) in the 450–750 nm region (Color figure online)

was selected as the excitation source to measure the emission spectra [5, 35, 38].

Figure 6 shows the emission spectra in the range of 450–750 nm for ZnP glasses doped with Sm^{3+} ions excited at 403 nm. As shown in Fig. 6, four main emission bands are observed at 562, 599, 646, and 707 nm [5]. These four bands are attributed to the emission transitions $^4G_{5/2} \rightarrow {}^6H_{P/2}$ ($P = 5,7,9,11$) [5, 23, 38–40]. Among these four emission transitions, the $^4G_{5/2} \rightarrow {}^6H_{7/2}$ transition has the highest intensity for all ZnP glasses [27]. The emission peak intensity of the Sm^{3+} ion-doped ZnP glasses varied with Sm^{3+} concentration. It reaches a maximum of 0.5 mol% and then gradually decreases with the samarium concentration. This might have occurred because of the concentration-quenching effect. At higher Sm^{3+} ion concentrations, non-radiative (NR) energy transfer occurs. Hence, the intensity of the emission peaks decreased. As presented in Table 2, the magnitude of the interionic distances (r_i) is 0.1SmZnP -4.231×10^{-7} Å; 0.5SmZnP -2.469×10^{-7} Å; 1.0SmZnP -1.961×10^{-7} Å; 1.5SmZnP -1.715×10^{-7} Å; and 2.0SmZnP -1.559×10^{-7} Å. With increasing Sm^{3+} ion concentration, the interionic distances (r_i) between the Sm^{3+} ions decrease [21, 23, 39]. Among all prepared ZnP glasses high and low inter-ionic distance (r_i) magnitudes were found to be 0.1SmZnP and 2.0SmZnP glass, respectively.

The stimulated emission cross-section (σ_P) is an important factor for the lasing efficiency of the preferred material [8, 39, 41] and is quantified for four transitions of the emission spectra using Eq. (7), as listed in Table 6. The $^4G_{5/2} \rightarrow {}^6H_{7/2}$ transition source offers a highly stimulated emission cross-section (σ_P) for all the ZnP glasses. Stimulated emission cross-section (σ_P) of the $^4G_{5/2} \rightarrow {}^6H_{7/2}$ transition of different concentrations of Sm^{3+} doped ZnP glasses had the values 11.34×10^{-22} (0.1 mol%), 19.26×10^{-22} (0.5 mol%), 18×10^{-22} (1.0 mol%), 17.11×10^{-22} (1.5 mol%), and 8.94×10^{-22} (2.0 mol%) cm^2, respectively. The stimulated emission cross-section (σ_P) of the Sm^{3+} ion-doped ZnP glass was found to have higher values at 0.5 mol% concentration and low values at 2.0 mol%.

Of these four transitions, the $^4G_{5/2} \rightarrow {}^6H_{7/2}$ transition has high branching ratio values for all ZnP glasses. For this transition, the values are 0.46, 0.48, 0.47, 0.46, and 0.45, respectively, as listed in Table 6. The stimulated emission cross-section (σ_P) of each transition increased up to 0.5 mol% Sm^{3+} and decreased further with increasing concentrations of Sm^{3+} ions [8].

3.7 Lifetime decay analysis

The decay profiles of the Sm^{3+} ions in ZnP glasses with different Sm^{3+} concentrations are shown in Fig. 7. The average lifetimes(τ_{avg}) were calculated

Table 6 Emission peak position (λ_p, nm), stimulated emission cross-sections ($\sigma_P \times 10^{-22} cm^2$), and experimental branching ratios (β_{exp}) of ZnP glasses doped with Sm^{3+} ions (0.1, 0.5, 1.0, 1.5, and 2.0 mol%)

Transitions	Peak position λ_p, nm	Emission cross-section $\sigma_P \times 10^{-22} cm^2$	Branching ratio β_{exp}
0.1SmZnP			
$^4G_{5/2} \rightarrow {}^6H_{5/2}$	562	10.98	0.07
$^4G_{5/2} \rightarrow {}^6H_{7/2}$	599	11.34	0.46
$^4G_{5/2} \rightarrow {}^6H_{9/2}$	646	06.62	0.37
$^4G_{5/2} \rightarrow {}^6H_{11/2}$	707	00.81	0.10
0.5SmZnP			
$^4G_{5/2} \rightarrow {}^6H_{5/2}$	562	17.34	0.06
$^4G_{5/2} \rightarrow {}^6H_{7/2}$	599	19.26	0.48
$^4G_{5/2} \rightarrow {}^6H_{9/2}$	646	10.29	0.37
$^4G_{5/2} \rightarrow {}^6H_{11/2}$	707	05.79	0.09
1.0SmZnP			
$^4G_{5/2} \rightarrow {}^6H_{5/2}$	562	16.44	0.06
$^4G_{5/2} \rightarrow {}^6H_{7/2}$	599	18.00	0.47
$^4G_{5/2} \rightarrow {}^6H_{9/2}$	646	09.98	0.37
$^4G_{5/2} \rightarrow {}^6H_{11/2}$	707	05.49	0.10
1.5SmZnP			
$^4G_{5/2} \rightarrow {}^6H_{5/2}$	562	15.52	0.06
$^4G_{5/2} \rightarrow {}^6H_{7/2}$	599	17.11	0.46
$^4G_{5/2} \rightarrow {}^6H_{9/2}$	646	09.59	0.36
$^4G_{5/2} \rightarrow {}^6H_{11/2}$	707	04.62	0.12
2.0SmZnP			
$^4G_{5/2} \rightarrow {}^6H_{5/2}$	562	07.53	0.07
$^4G_{5/2} \rightarrow {}^6H_{7/2}$	599	08.94	0.45
$^4G_{5/2} \rightarrow {}^6H_{9/2}$	646	05.51	0.35
$^4G_{5/2} \rightarrow {}^6H_{11/2}$	707	02.29	0.13

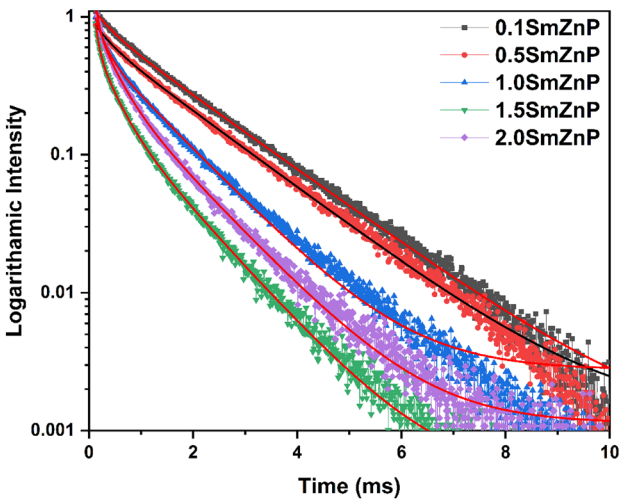

Fig. 7 Fitted decay profiles of $^4G_{5/2} \rightarrow {}^6H_{7/2}$ level for zinc phosphate (ZnP) glasses doped with Sm^{3+} ions (0.1, 0.5, 1.0, 1.5, and 2.0 mol%) (Color figure online)

using the equation from the literature [42], The average lifetimes (τ_{avg}) of each glass prepared are 1.52 ms (0.1 mol%), 1.47 ms (0.5 mol%), 0.96 ms (1.0 mol%), 0.63 ms (1.5 mol%), and 0.60 ms (2.0 mol%) for different concentrations of samarium. The results show that the average lifetime (τ_{avg}) decreases with increasing Sm^{3+} concentration by enhancing the energy transfer between Sm^{3+} ions.

3.8 Colorimetry

Figure 8 shows the chromaticity diagram for different concentrations of Sm^{3+} ions in the ZnP glasses. One can see that as the concentration of samarium increased, the color disparities from orange to reddish-orange. Equations (8), and (9) were used to calculate color coordinate temperatures (CCT) and color purity (CP) for Sm^{3+} ions doped in different ZnP glasses. Table 7 presents the results of this study.

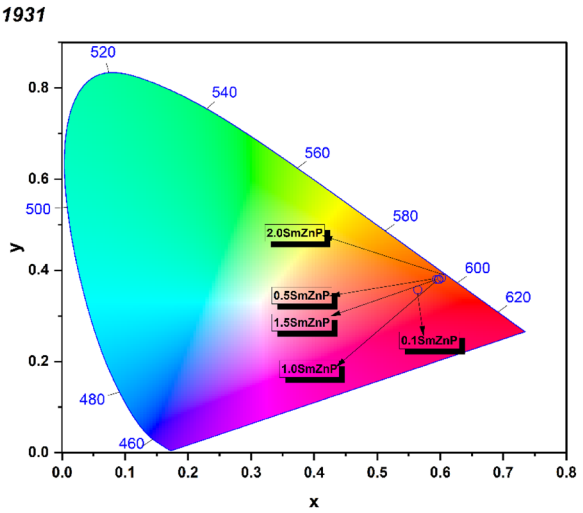

Fig. 8 CIE 1931 chromaticity color coordinates of zinc phosphate (ZnP)glasses doped with Sm^{3+} ions (0.1, 0.5, 1.0, 1.5, and 2.0 mol%) (Color figure online)

Table 7 CIE 1931 color coordinates (x_c, y_c), correlated color temperature (CCT, K) and color purity (CP, %) of ZnP glasses doped with Sm^{3+} ions (0.1, 0.5, 1.0, 1.5, and 2.0 mol%)

Sample	Color coordinates		CCT	CP
	x_c	y_c	K	(%)
0.1SmZnP	0.564	0.357	1744	80.5
0.5SmZnP	0.598	0.380	1752	91.6
1.0SmZnP	0.597	0.380	1750	90.2
1.5SmZnP	0.602	0.384	1748	90.2
2.0SmZnP	0.594	0.380	1742	90.2

CCT values vary from 1741 to 1752 K and CP varies from 80.5 to 91.6%, while the present glasses fall in the candle flame range (from 1000 to 2000 K). Among the prepared ZnP glasses, the 0.5SmZnP glass had the highest CCT value (1752 K) and the highest color purity (91.6%). Therefore, the prepared 0.5SmZnP glass may be beneficial for reddish-orange lighting applications such as display panels, bio-friendly light sources, microbeam radiotherapy, cathode-ray tubes (CRT), and plasma displays [43].

4 Conclusion

The melt-quenching method was used to prepare various concentrations of Sm^{3+} ion-doped ZnP glasses with compositions of (60-x) P_2O_5–20ZnO–10LiF–10SrO–xSm_2O_3, where x = (0.1, 0.5, 1.0, 1.5, and 2.0). From the XRD profiles, the ZnP glasses were determined to be amorphous. The FTIR spectra of the ZnP glasses showed vibrational bands corresponding to characteristic phosphate groups. To evaluate the optical absorption spectra empirically, J–O theory was applied, and the intensity parameters were calculated. Ω_4 showed higher values compared to the other intensity parameters Ω_2 and Ω_6, for all ZnP glasses doped with Sm^{3+}ions. Low Ω_2 values denote low covalency and low asymmetry, whereas high Ω_4 values reflect the stiffness of the related host glass.

At an emission wavelength of λ_{emi} = 599 nm, ten excitation bands were seen in the excitation spectra, and at an excitation wavelength of λ_{exc} = 403 nm, four bands were attributed to the emission transitions $^4G_{5/2} \rightarrow {}^6H_{P/2}$ (P = 5, 7, 9, 11). Among the four emission transitions, the $^4G_{5/2} \rightarrow {}^6H_{7/2}$ transition emitted reddish-orange light at a wavelength of 599 nm. Among the present glasses, 0.5SmZnP glass was found to have a higher Quality factor (χ) of 1.31 and a high stimulated emission cross-section (σ_P) of 19.26×10^{-22} cm^2 for the $^4G_{5/2} \rightarrow {}^6H_{7/2}$ transition. The quality factor (χ), stimulated emission cross-section (σ_P) values, and CIE1931 color coordinates show that ZnP glasses doped with Sm^{3+} ions are practical candidates for reddish-orange laser media. Based on the above results, it was concluded that SmZnP glass doped with 0.5 mol% Sm^{3+} ions (0.5SmZnP) can be used for the development of cathode-ray tubes (CRT), and plasma displays.

Acknowledgements

One of the authors, S. Vidya Sagar, thanks the government's funding agency, the University Grants Commission (UGC), Govt. of India, New Delhi, for providing financial support in the form of a Junior Research Fellowship (JRF) under UGC-CSIR NET-JRF (No. F. 82-1/2018(SA-III), and UGC-Ref. No.191620143937, issued on 05/20/2020, which enabled him to conduct this research. The authors thank Mr. Essaki Kumar, a laboratory technician at CIF Pondicherry University, who helped obtain excitation, emission, and lifetime data; the Faculty of Physics and Chemistry at Yogi Vemana University for facilitating the instrumentation of XRD and FTIR, and the Faculty of Physics at Sri Venkateshwara University for facilitating the instrumentation of the UV-VIS-NIR spectrometer.

Author contributions

SVS: conceptualization, methodology, validation, investigation, writing-original draft preparation, visualization, SB: conceptualization, investigation, writing-review & editing, visualization, KVR: conceptualization, investigation, writing-review & editing, supervision.

Funding

This study was supported by the government's funding agency, the University Grants Commission (UGC), Government of India, New Delhi, in the form of a Junior Research Fellowship (JRF) under UGC-CSIR NET-JRF, No.F.82–1/2018(SA-III), UGC-Ref. No.: 191620143937, issued on 05/20/2020 to S. Vidya Sagar.

Data availability

Data will be made available on reasonable request.

Declarations

Competing interests The authors declared that they have no relevant financial or non-financial interests to disclose.

References

1. F. Ahmadi, R. Hussin, S.K. Ghoshal, Optik (Stuttg) **227**, 166000 (2021). https://doi.org/10.1016/j.ijleo.2020.166000
2. M.K.K. Poojha, K. Marimuthu, P.E. Teresa, N. Almousa, M.I. Sayyed, Nucl. Eng. Technol. **54**, 3841 (2022). https://doi.org/10.1016/j.net.2022.05.006
3. F. Afaneh, Z.Y. Khattari, M.S. Al-Buriahi, J. Market. Res. **19**, 3788 (2022). https://doi.org/10.1016/j.jmrt.2022.06.125
4. S.A.M. Issa, H.M.H. Zakaly, H.O. Tekin, H.A. Saudi, A. Badawi, M. Pyshkina, G. Susoy, A.I. Elazaka, A. Ene, Nanomaterials **11**, 1713 (2021). https://doi.org/10.3390/nano11071713
5. P. Li, X. Zhang, J. Zhang, X. Qi, X. Liu, Coatings **12**, 3 (2022). https://doi.org/10.3390/coatings12010003
6. S.N. Rasool, S. Shabeena, C.R. Kesavulu, S. Babu, J. Mater. Sci. Mater. Electron. **33**, 19263 (2022). https://doi.org/10.1007/s10854-022-08764-y
7. B. Sengthong, H. Van Tuyen, N.T.T. An, P. Van Do, N.T.Q. Hai, P.T.M. Chau, V.X. Quang, J. Electron. Mater. **47**, 2316 (2018). https://doi.org/10.1007/s11664-017-6056-x
8. S. Hussain, R.J. Amjad, B.M. Walsh, H. Mehmood, N. Akbar, F. Alvi, M.R. Dousti, A. Sattar, A. Iqbal, S. Hussain, Y. Li, Solid State Commun. **298**, 113632 (2019). https://doi.org/10.1016/j.ssc.2019.05.003
9. H. Tiwari, C.C. Dhondiyal, In Mater. Today Proc. **47**, 1682 (2021). https://doi.org/10.1016/j.matpr.2021.05.493
10. M.A. Farag, A. Ibrahim, M.Y. Hassaan, R.M. Ramadan, J. Aust. Ceram. Soc. **58**, 653 (2022). https://doi.org/10.1007/s41779-022-00716-3
11. A. Okasha, M.S. Gaafar, S.Y. Marzouk, J. Mater. Sci. Mater. Electron. **34**, 354 (2023). https://doi.org/10.1007/s10854-022-09677-6
12. S.A. Ansari, M.O. Ansari, A. Alshahrie, M. Shahadat, N. Parveen, R. Darwesh, S.F. Aboushoushah, Appl. Sci. (Switzerland) **12**, 2632 (2022). https://doi.org/10.3390/app12052632
13. S.Y. Marzouk, H.M. Elsaghier, W. Abbas, N.A. Zidan, M.A. Azooz, Results Chem. **4**, 100395 (2022). https://doi.org/10.1016/j.rechem.2022.100395
14. M.A. Marzouk, H.A. ElBatal, Y.M. Hamdy, F.M. Ezz-Eldin, Int. J. Opt. (2019). https://doi.org/10.1155/2019/6527327
15. K.S. Lim, N. Vijaya, C.R. Kesavulu, C.K. Jayasankar, Opt. Mater. (Amst) **35**, 1557 (2013). https://doi.org/10.1016/j.optmat.2013.03.026
16. V.M. Krishna, S. Mahamuda, P.R. Rani, K. Swapna, M. Venkateswarlu, A.S. Rao, Opt. Mater. (Amst). **109**, 110368 (2020). https://doi.org/10.1016/j.optmat.2020.110368
17. S. Hussain, R.J. Amjad, M. Tanveer, M. Nadeem, H. Mahmood, A. Sattar, A. Iqbal, I. Hussain, Z. Amjad, S.Z. Hussain, S.A. Siddique, M.R. Dousti, Glass Phys. Chem. **43**, 538 (2017). https://doi.org/10.1134/S1087659617060219
18. A. El-Adawy, R. El-Mallawany, H.A. Elabd, I.A. El-Mesady, Results Opt. **8**, 100234 (2022). https://doi.org/10.1016/j.rio.2022.100234
19. A. Okasha, A.M. Abdelghany, S.K. Mohamed, S.Y. Marzouk, H.A. El-Batal, M.S. Gaafar, J. Mater. Sci. Mater. Electron. **29**, 20907 (2018). https://doi.org/10.1007/s10854-018-0234-3
20. H.M.H. Zakaly, Y.S. Rammah, H.O. Tekin, A. Ene, A. Badawi, S.A.M. Issa, J. Market. Res. **18**, 1424 (2022). https://doi.org/10.1016/j.jmrt.2022.03.030

21. M. Rajesh, E. Kavaz, D.P.B. Raju, Mater. Res. Bull. **142**, 111383 (2021). https://doi.org/10.1016/j.materresbull.2021.111383
22. Y.A. Yamusa, Y. Musa, M. Tufail, A.A. Sa'id, A. Isma'ila, A.U. Abubakar, I. Bulus, Optik (Stuttg) **267**, 169710 (2022). https://doi.org/10.1016/j.ijleo.2022.169710
23. L. Fernández-Rodríguez, R. Balda, J. Fernández, A. Durán, M.J. Pascual, Int. J. Appl. Glass Sci. **14**, 140 (2022). https://doi.org/10.1111/ijag.16584
24. I. Ataullah, S. Khan, M. Khattak, J. Shoaib, I. Kaewkhao, G. Rooh, J. Alloys Compd. **875**, 160095 (2021). https://doi.org/10.1016/j.jallcom.2021.160095
25. D. Bayoudhi, C. Bouzidi, E. Matei, M. Secu, A. Catalin Galca, J. Lumin. **265**, 120204 (2024). https://doi.org/10.1016/j.jlumin.2023.120204
26. G. Lakshminarayana, A.N. Meza-Rocha, O. Soriano-Romero, E.F. Huerta, U. Caldiño, A. Lira, D.E. Lee, J. Yoon, T. Park, J. Alloys Compd. **884**, 161076 (2021). https://doi.org/10.1016/j.jallcom.2021.161076
27. P. Sailaja, S. Mahamuda, K. Swapna, M. Venkateswarlu, A.S. Rao, Mater. Sci. Eng. B Solid State Mater. Adv. Technol. **270**, 115198 (2021). https://doi.org/10.1016/j.mseb.2021.115198
28. D.S. Raju, S.H. Bindu, M. Rajesh, J.S. Krishna, V.V. Krishna, B.D. Prasad Raju, C.L. Raju, J. Lumin. **252**, 119292 (2022). https://doi.org/10.1016/j.jlumin.2022.119292
29. N. Ravina, V. Sheetal, S. Kumar, N. Dahiya, R.P. Deopa, A.S. Rao, J. Lumin. **229**, 117651 (2021). https://doi.org/10.1016/j.jlumin.2020.117651
30. A. Alimuddin, M. Rafeeq, Orient. J. Chem. **37**, 177 (2021). https://doi.org/10.13005/ojc/370124
31. W.T. Carnall, P.R. Fields, K. Rajnak, J. Chem. Phys. **49**, 4424 (1968). https://doi.org/10.1063/1.1669893
32. M. Kumar, H. Nagabhushana, Y.C. Ratnakaram, J. Non Cryst. Solids **573**, 121146 (2021). https://doi.org/10.1016/j.jnoncrysol.2021.121146
33. J. Bhemarajam, M. Swapna, P.M. Babu, P.S. Prasad, Opt. Mater. (Amst). **113**, 110818 (2021). https://doi.org/10.1016/j.optmat.2021.110818
34. S.B. Mallur, T.C. Khoo, S. Rijal, O.R. Huff, P.K. Babu, Mater. Chem. Phys. **258**, 123886 (2021). https://doi.org/10.1016/j.matchemphys.2020.123886
35. N. Kiwsakunkran, N. Chanthima, J. Kaewkhao, N. Sangwaranatee, Mater. Today Proc. **43**, 2554 (2021). https://doi.org/10.1016/j.matpr.2020.04.616
36. I. Ullah, I. Khan, S.K. Shah, S.A. Khattak, M. Shoaib, J. Kaewkhao, T. Ahmad, E. Ahmed, G. Rooh, A. Khan, J. Lumin. **230**, 117700 (2021). https://doi.org/10.1016/j.jlumin.2020.117700
37. R. Cao, J. Wei, T. Chen, B. Lan, L. Li, R. Liu, Z. Luo, J. Wang, J. Mol. Struct. **1274**, 134404 (2023). https://doi.org/10.1016/j.molstruc.2022.134404
38. R. Cao, J. Lin, B. Lan, F. Cheng, T. Chen, L. Li, R. Liu, J. Wang, J. Mol. Struct. **1282**, 135221 (2023). https://doi.org/10.1016/j.molstruc.2023.135221
39. N. Kiwsakunkran, N. Chanthima, H. Kim, J. Kaewkhao, Phys. Status Solidi **43**, 2554 (2022). https://doi.org/10.1002/pssa.202200437
40. J. Dahiya, A. Hooda, A. Agarwal, S. Khasa, Opt. Mater. (Amst) **134**, 113162 (2022). https://doi.org/10.1016/j.optmat.2022.113162
41. K.S. Rudramamba, D.V. Krishna Reddy, T. Sambasiva Rao, S.K. Taherunnisa, N. Veeraiah, M. Rami Reddy, Opt. Mater. (Amst) **89**, 68 (2019). https://doi.org/10.1016/j.optmat.2018.12.048
42. L. Sumrall, L. Smith, E. Alhatmi, Y. Chmykh, D. Mitchell, J. Nadeau, BBA Adv. **3**, 100088 (2023). https://doi.org/10.1016/j.bbadva.2023.100088
43. J. Rajagukguk, R. Situmorang, B. Nasution, D.H. Rajagukguk, R.M.I. Retno Susilorini, C.S. Sarumaha, J. Kaewkhao, J. Phys. Conf. Ser. **1811**(1), 012112 (2021). https://doi.org/10.1088/1742-6596/1811/1/012112

Publisher's Note Springer Nature remains neutral with regard to jurisdictional claims in published maps and institutional affiliations.

Springer Nature or its licensor (e.g. a society or other partner) holds exclusive rights to this article under a publishing agreement with the author(s) or other rightsholder(s); author self-archiving of the accepted manuscript version of this article is solely governed by the terms of such publishing agreement and applicable law.